Simultaneous Measurements of Atmospheric Water Vapor with MIR, Raman Lidar, and Rawinsondes

J. R. WANG, S. H. MELFI, P. RACETTE, AND D. N. WHITEMEN

NASA/Goddard Space Flight Center, Greenbelt, Maryland

L. A. CHANG

Futuretech Corp., Gaithersburg, Maryland

R. A. FERRARE AND K. D. EVANS

Hughes STX Corporation, Lanham, Maryland

F. J. SCHMIDLIN

NASA/Wallops Flight Facility, GSFC, Wallops Island, Virginia

(Manuscript received 11 May 1994, in final form 19 November 1994)

ABSTRACT

Simultaneous measurements of atmospheric water vapor were made by the Millimeter-wave Imaging Radiometer (MIR), Raman lidar, and rawinsondes. Two types of rawinsonde sensor packages (AIR and Vaisala) were carried by the same balloon. The measured water vapor profiles from Raman lidar, and the Vaisala and AIR sondes were used in the radiative transfer calculations. The calculated brightness temperatures were compared with those measured from the MIR at all six frequencies (89, 150, 183.3 ± 1, 183.3 ± 3, 183.3 ± 7, and 220 GHz). The results show that the MIR-measured brightness temperatures agree well (within ±2 K) with those calculated from the Raman lidar and Vaisala measurements. The brightness temperatures calculated from the AIR sondes differ from the MIR measurements by as much as 10 K, which can be attributed to low sensitivity of the AIR sondes at relative humidity less than 20%. Both calculated and the MIR-measured brightness temperatures were also used to retrieve water vapor profiles. These retrieved profiles were compared with those measured by the Raman lidar and rawinsondes. The results of these comparisons suggest that the MIR can measure the brightness of a target to an accuracy of at most ±2 K and is capable of retrieving useful water vapor profiles.

1. Introduction

Water vapor is one of the key components affecting the atmospheric processes over a wide range of temporal and spatial scales from global climate to micrometeorology (Lindzen 1990; Haydu and Krishnamurti 1981; Elliot and Gaffen 1991). It provides inputs to numerical weather prediction and weather studies because the latent heat release due to condensation is crucial to the evolution of many weather systems (Haydu and Krishnamurti 1981). Its enhancement in the cloudy areas may have a large impact on the development of precipitation in the first hours of a model forecast (Turpeinen et al. 1990). The distribution of total precipitable water over the ocean surface can also be considered as a tracer of the atmospheric motions (Prabhakara et al. 1979). All these considerations point to the need for frequent and efficient measurements of the global distribution of atmospheric water vapor.

Measurements of atmospheric water vapor vary from single locations (e.g., rawinsondes, ground-based Raman lidar) to aircraft flights at regional scales, and to satellite coverage over the entire globe. A number of different methods have been used for these measurements. The satellite large-scale measurements have been made by either infrared (e.g., TOVS, the TIROS Operational Vertical Sounder) or microwave sensors (e.g., SSM/I, the Special Sensor Microwave/Imager). The TOVS measurements provide water vapor concentrations at several altitude levels, but the SSM/I measurements give only the distribution of total precipitable water over the ocean areas (Alishouse et al. 1990). More recently, a five-channel microwave humidity sounder (SSM/T-2, Special Sensor Microwave/

Corresponding author address: Dr. James R. Wang, NASA/Goddard Space Flight Center, Code 975, Greenbelt, MD 20771.

Temperature-2) was placed aboard the DMSP (Defense Meteorological Satellite Project) F-11 satellite to estimate water vapor profiles globally (Falcone et al. 1993). At aircraft altitudes, a number of measurements have been made previously with both infrared and microwave humidity sounders (Wang et al. 1983; Wang and Chang 1990; Wang et al. 1993; Kakar 1983; Kakar and Lambrigtsen 1984; Smith et al. 1986) to develop the algorithms for retrieval of water vapor profiles. These studies based on the aircraft measurements have shown reasonable success and strongly suggest the soundness of both infrared and microwave approaches for large-scale water vapor profiling.

In this paper we compare the results of near-simultaneous measurements from a ground-based Raman lidar system, a six-channel airborne Millimeter-wave Imaging Radiometer (MIR), and two different rawinsonde sensor packages (AIR and Vaisala). The lidar system has been in operation for the past several years at a few different locations (Whiteman et al. 1992a; Whiteman et al. 1992b; Melfi et al. 1989; Ferrare et al. 1993), while the MIR was a newly developed instrument (Racette et al. 1992; Racette et al. 1994) that was flown for the first time in California aboard the NASA (National Aeronautics and Space Administration) ER-2 aircraft in May 1992. The rawinsonde observations with different sensor packages were quite often not in agreement with one another, as previously reported by Melfi et al. (1989). The inaccuracy in the rawinsonde data could cause severe problems for the users, especially when used to understand radiative transfer. The results of using the different rawinsonde datasets for radiative transfer calculations and for comparisons with measurements from various MIR frequency channels are discussed in detail. Retrievals of water vapor profiles from both MIR-measured and simulated datasets were performed and results were compared with Raman lidar and rawinsonde measurements. A sensitivity study of the MIR with respect to the rawinsonde observations was reported recently by Jackson and Gasiewski (1995).

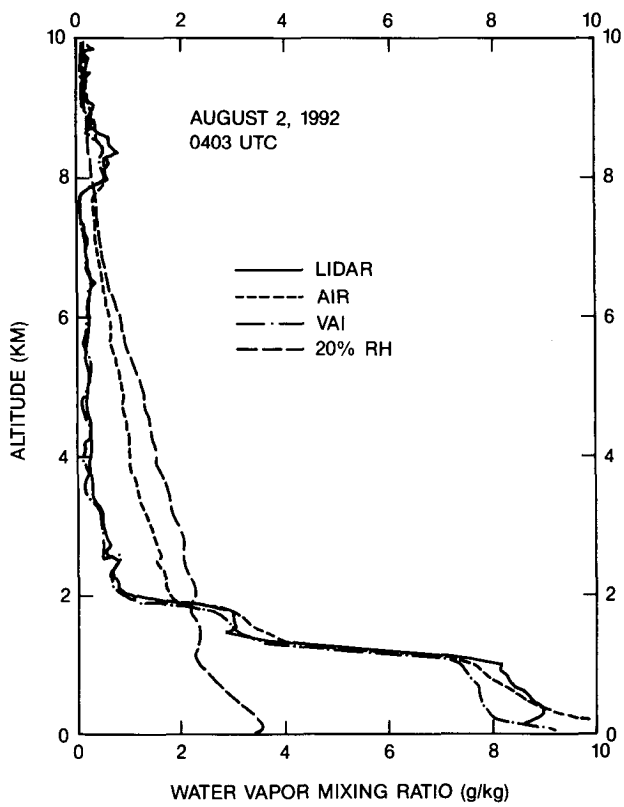

FIG. 1. The variations with height of the water vapor mixing ratios measured by the ground-based Raman lidar system and three different rawinsondes on the same balloon.

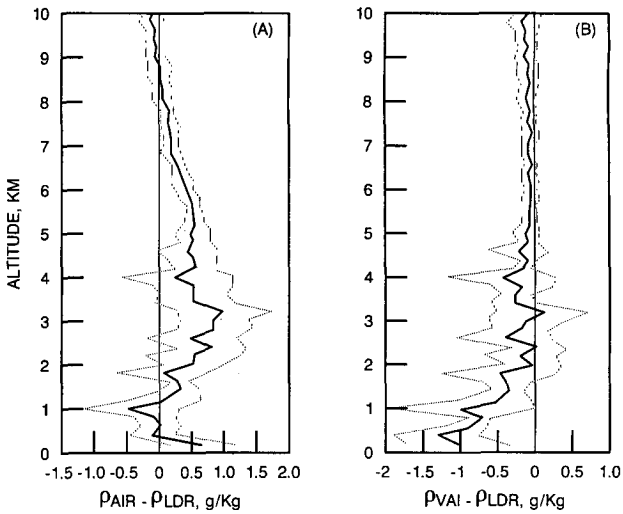

FIG. 2. The variations with height of the average mixing ratio differences (solid curves) and their standard deviations (dotted curves) derived from measurements of (a) Raman lidar and AIR sondes and (b) Raman lidar and Vaisala sondes.

2. Measurements

The measurements were conducted at the NASA Goddard Space Flight Center's (GSFC) Wallops Flight Facility (WFF) in Wallops Island, Virginia, under a joint program of ATMIS-II (Atmospheric Moisture Intercomparison Studies II) and SSM/T-2 sensor validation. The sensor packages deployed at the WFF include the airborne MIR, ground-based Raman lidar system, and the AIR and Vaisala sondes. A previous intercomparison study, ATMIS-I, was also conducted at the WFF in April 1989 with the ground-based low-frequency microwave radiometers and Raman lidar, and rawinsondes (England et al. 1992). The results of the SSM/T-2 validation have been reported by Falcone et al. (1993).

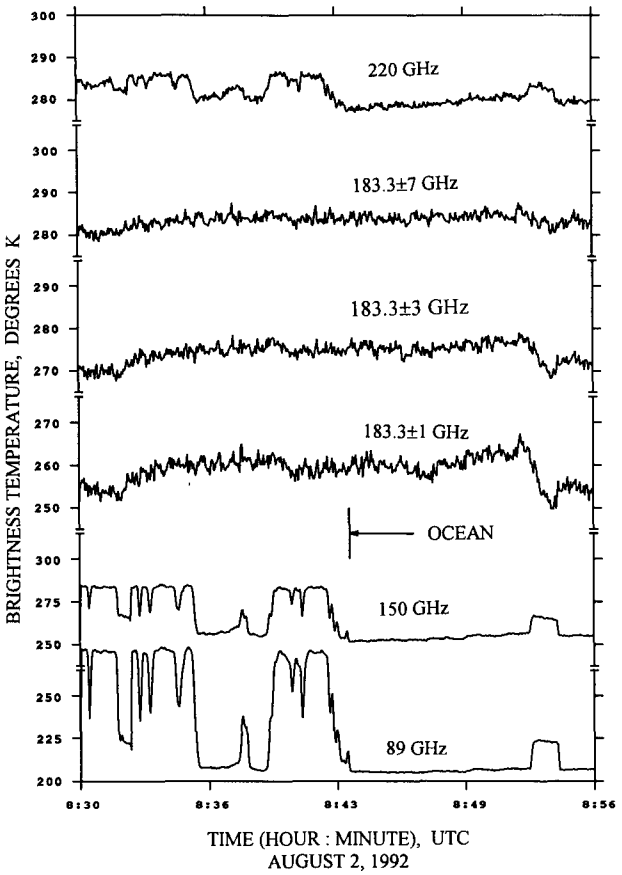

FIG. 3. Variations of brightness temperatures over land and ocean measured by the six channels of MIR near NASA/GSFC Wallops Flight Facility.

The GSFC scanning Raman lidar used for these measurements, described by Whiteman et al. (1992a) and Ferrare et al. (1992), incorporated many new features and was significantly improved over a previous system, described by Melfi and Whiteman (1985), Melfi et al. (1989), England et al. (1992), and Whiteman et al. (1992b). This lidar is a trailer-based system that uses an XeF laser to transmit light at 351 nm. The combined aerosol and molecular backscattered light at the laser wavelength is detected as well as Raman scattered light from water vapor (403 nm), nitrogen (383 nm), and oxygen (372 nm) molecules. Profiles of the water vapor mixing ratio are computed from the ratio of Raman scattering by water vapor to Raman scattering by nitrogen. These profiles are calibrated using a weighted least squares regression of the lidar ratios to the water vapor mixing ratios measured by coincident rawinsondes launched at the lidar site. Rawinsonde data below 30% relative humidity are not used because of potential unreliable rawinsonde moisture measurements in dry conditions (Wade and Wolfe 1989; Garand et al. 1992). For a 1-min profile, the random error in these profiles is less than 10% for altitudes below 7.5–8.5 km. By averaging for longer periods of time, and/or by reducing the vertical resolution, profiles above 8.5 km can be obtained (Soden et al. 1994).

The MIR is a newly built six-frequency (89, 150, 183.3 ± 1, 183.3 ± 3, 183.3 ± 7, and 220 GHz) cross-track-scanning total-power radiometer mounted onboard the NASA ER-2 aircraft. The design and fabrication of the instrument are a joint effort between Goddard Space Flight Center and Georgia Institute of Technology (Racette et al. 1992; Racette et al. 1994). The sensor has a 3-dB beamwidth of about 3.5° at all frequency channels and covers an angular swath of ±50° with respect to nadir. In every scanning cycle, it also views two external calibration targets; one of them is heated to a temperature of approximately 330 K and another remains at the ambient temperature that, at the cruising altitude of the ER-2 aircraft, is about 240 K. The temperatures of these calibration targets are closely monitored to within ±0.1 K. The temperature sensitivity of this sensor is on the order of 0.4 K and the calibration accuracy is better than ±2 K in the brightness temperature range of 240–300 K (Racette et al. 1994). The measurement accuracy below 240 K is somewhat uncertain; based on the calibration studies in the laboratory, the accuracy near the liquid nitrogen temperature of 77 K is estimated to be ±3 K (Racette et al. 1994).

Two types of rawinsonde sensor packages (AIR and Vaisala) were launched during the lidar–radiometer measurements. Balloons carrying both types of rawinsondes were launched in 3-h intervals during the measurement period of 0100–0700 UTC on each of these five nights. The humidity sensors from the AIR sondes were made of carbon resistive strips that had a low measurement limit near 20%–30% because of the algorithm used. Those on the Vaisala sondes were made of capacitive thin-films; the relative humidities reported by the Vaisala sensors were generally lower than those provided by the AIR sondes.

The simultaneous measurements of all these sensors were conducted on five nights between 2100 and 0500 LT (0100–0900 UTC) during the period of 29 July–6 August 1992. In the first four days of measurements on 29–30 July and 2–3 August, the sky was mostly clear; while on the last day of measurements on 6 August, there was heavy cloud cover at WFF. During the almost 8-h operation, the Raman lidar was operated nearly continuously and rawinsonde launches were generally made at 2100, 1200, and 0300 LT. The ER-2 aircraft spent about 2 h over the lidar and rawinsonde sites in each of these five nights. Three flights on 29–30 July and 6 August lasted about 6 h because of the additional activities associated with the MIR validation/calibration of the DMSP's SSM/T-2 sensor (Falcone et al. 1993). The flight pattern over the WFF

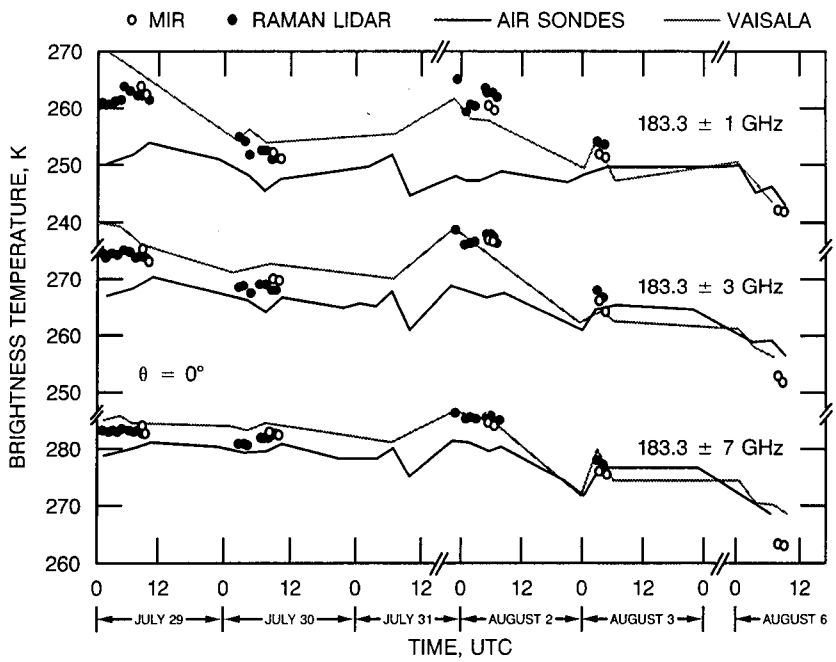

FIG. 4. A comparison of the brightness temperatures measured by the MIR at 183.3 ± 1, 183.3 ± 3, and 183.3 ± 7 GHz with those calculated from the measurements of Raman lidar, AIR sonde, and Vaisala sonde.

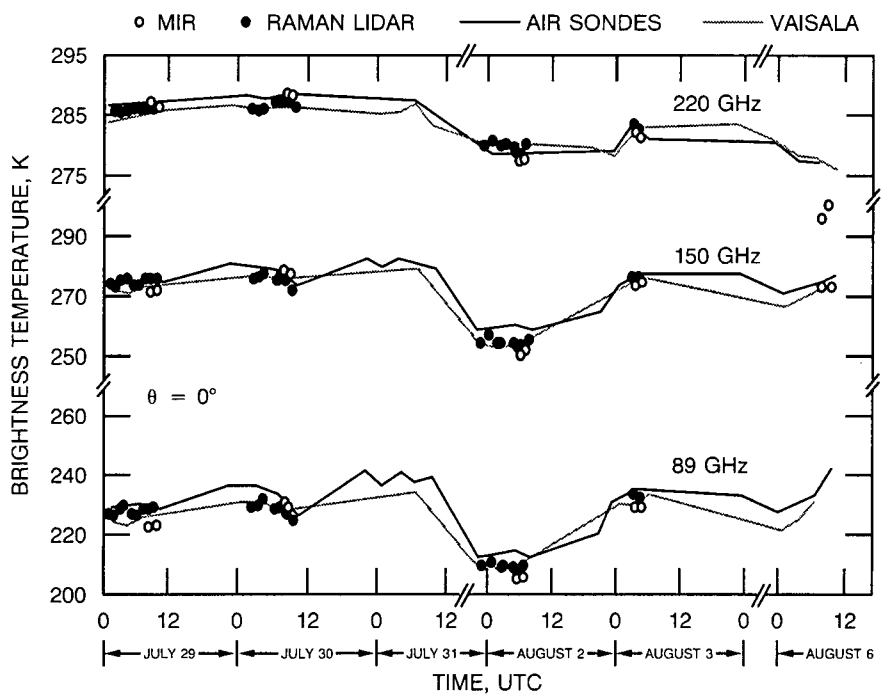

FIG. 5. A comparison of the brightness temperatures measured by the MIR at 89, 150, and 220 GHz with those calculated from the measurements of Raman lidar, AIR sonde, and Vaisala sonde.

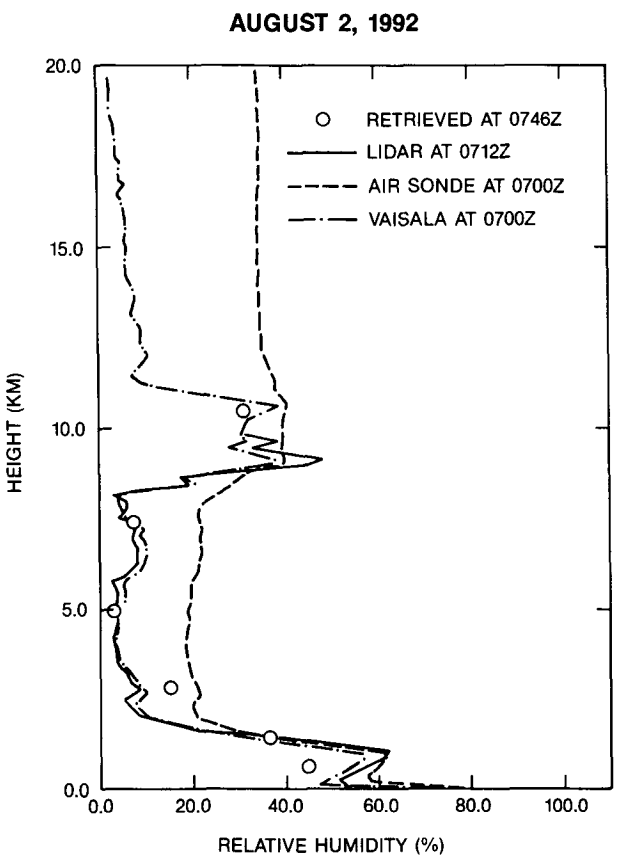

FIG. 6. A comparison of the relative humidity profile retrieved from the MIR measurements with those measured by the Raman lidar, AIR sonde and Vaisala sonde on 2 August 1992.

area was the same for all five nights. After reaching the cruising altitude of about 20 km, the ER-2 aircraft flew four flight lines. Two of the flight lines were over water just off the coast and parallel to the coast line along the direction of south-southwest and north-northeast. The other two flight lines were over the lidar site and perpendicular to the coast line along the direction of west-northwest and east-southeast. MIR performed well in each of these flights.

3. Results

The results of a typical water vapor measurement comparison from the ground-based Raman lidar and the three different rawinsondes are given in Fig. 1. The figure shows the altitude variation of the water vapor mixing ratios on the night of 2 August 1992. A curve showing the mixing ratio ρ for 20% relative humidity is also included in the figure for comparison. The sky over the region of WFF was clear and there were no observable patches of clouds within the range of the Raman lidar (a hemisphere of about 10 km in radius). At altitudes less than 2 km, the lidar and AIR sonde mixing ratios are in good agreement, while the Vaisala mixing ratios are generally lower at altitudes less than 1 km. The measurements from Raman lidar and Vaisala sondes agree very well at altitudes greater than 2 km, while that from the AIR sondes give generally higher ρ values because of the AIR sonde limitation in sensitivity to low relative humidities.

The discrepancies in the measurements by the different sensors displayed in Fig. 1 are not unique just for the night of 2 August 1992. They are persistent for all five nights of observations. To illustrate this, the differences in the pairs of simultaneous ρ measurements by AIR and Raman lidar and by Vaisala sondes and Raman lidar are taken and their averages and standard deviations calculated. The results are shown in Figs. 2a and 2b respectively, for the height variations of the averages (solid curves) and standard deviations (dotted curves) of the mixing ratio differences $\rho_{air} - \rho_{ldr}$ and $\rho_{vai} - \rho_{ldr}$. The subscripts in ρ's identify the type of measurements (AIR, Vaisala, or lidar). At altitudes less than 2 km, the mean $\rho_{air} - \rho_{ldr}$ value is close to 0, while the mean $\rho_{vai} - \rho_{ldr}$ is about -0.5 to -1.0 g kg^{-1}. At altitudes greater than 2 km, the mean $\rho_{air} - \rho_{ldr}$ is

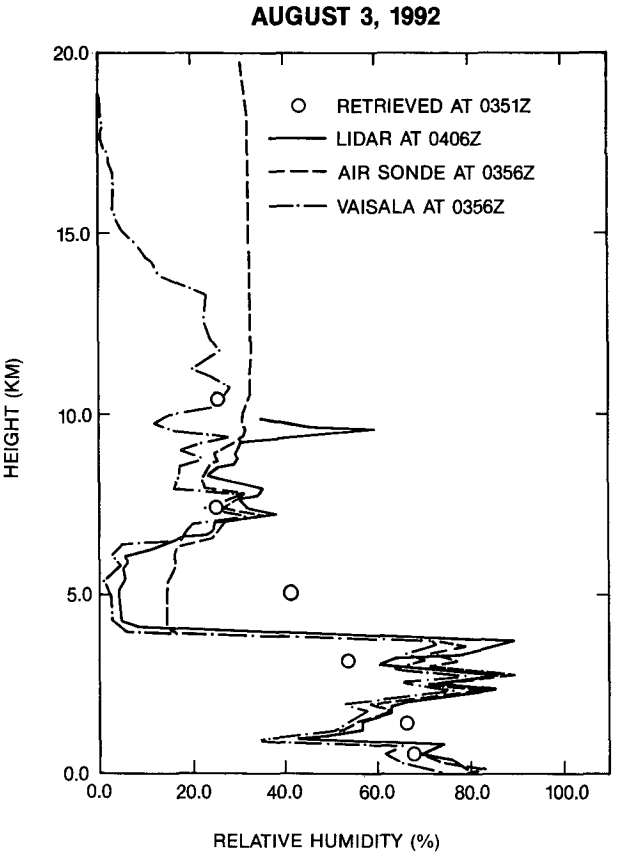

FIG. 7. A comparison of the relative humidity profile retrieved from the MIR measurements with those measured by the Raman lidar, AIR sonde, and Vaisala sonde on 3 August 1992.

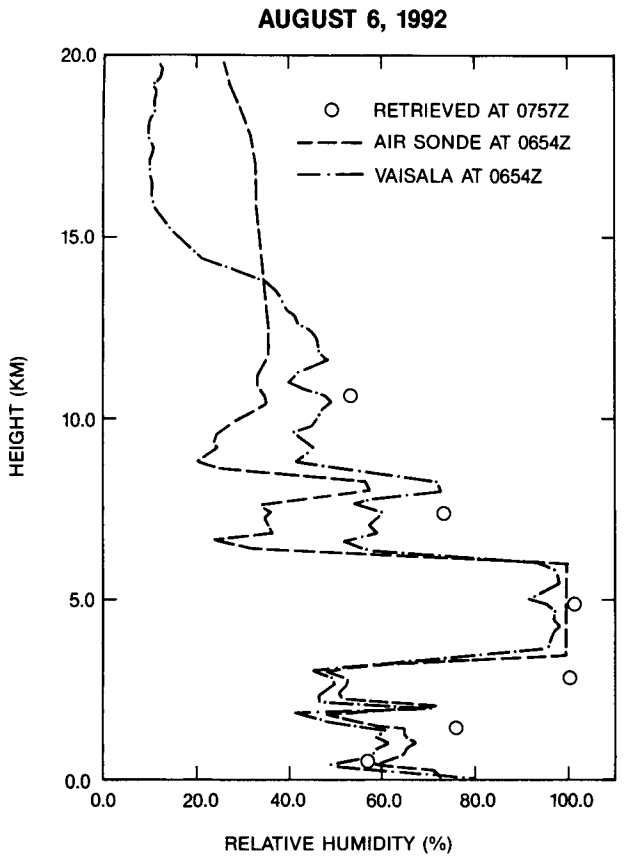

FIG. 8. A comparison of the relative humidity profile retrieved from the MIR measurements with those measured by the AIR sonde and Vaisala sonde on 6 August 1992.

approximately 0.5 g kg^{-1}, while the mean $\rho_{vai} - \rho_{ldr}$ is close to 0. These features reflect the persistent differences in the measurements among the different humidity sensors, which turn out to be important in the radiative transfer calculations and the comparison with the MIR measurements. The differences between the AIR and Vaisala sondes are likely caused by the algorithms applied to the measured parameters in the derivation of relative humidities (Schwarz and Doswell 1991).

Figure 3 shows a typical example of the variations of brightness temperatures measured by the six channels of MIR on 2 August 1992 as the ER-2 aircraft flew from the west-northwest to the east-southeast along a flight track directly over WFF and nearly perpendicular to the coast line. The measurements at the times later than about 0843 UTC are over the ocean areas east of WFF. The measurements before this time are over both land and water surfaces west of the WFF coast line. The atmosphere is opaque to the three water vapor channels near 183 GHz and completely shields surface emission at these frequencies. The atmosphere is more transparent to the other three window channels at 89, 150, and 220 GHz, and the surface features are readily observable by the MIR at these frequencies. Over the ocean areas, the T_b values measured by the MIR's 89-, 150-, and 220-GHz channels are approximately 206, 250, and 280 K, respectively. Over the land surface, the measured T_b values are, following the same channel sequence, approximately 280, 285, and 287 K. The maximum T_b values observed by these window channels near the time of about 0854 UTC are signatures of cloud cover over the ocean surface.

To compare the experimental results from different sensors, we compute the upwelling brightness temperatures, for nadir viewing at the six frequencies of the MIR, from the Raman lidar and rawinsonde data by the radiative transfer equation (Schaerer and Wilheit 1979; Wang and Chang 1990):

$$T_b = \int_0^\infty e^{-\tau(h,\,\infty)}\gamma(\nu, h)T(h)dh + e^{-\tau(0,\,\infty)} \times [\epsilon_s T_{surf} + (1 - \epsilon_s)\int_0^\infty e^{-\tau(0,\,h)}T(h)\gamma(\nu, h)dh] + (1 - \epsilon_s)e^{-2\tau(0,\,\infty)}T_{CB}, \quad (1)$$

where

$$\tau(z, y) = \int_z^y \gamma(\nu, x)dx \quad (2)$$

represents the optical depth between heights z and y. The term ϵ_s is the emissivity of the surface, $\gamma(\nu, h)$ the absorption coefficient of the atmosphere at height h and frequency ν, $T(h)$ the temperature profile of the atmosphere, T_{surf} the thermometric temperature of the surface, and T_{CB} the 2.7-K cosmic background temperature.

In the calculations of $\gamma(\nu, h)$, the upgraded version of the millimeter-wave propagation model of Liebe (1985, 1989) is adopted. The model covers all the absorption lines up to the frequency of 1000 GHz. It can be shown that the contribution to $\gamma(\nu, h)$ from absorption lines above 1000 GHz is negligibly small and can be ignored in the calculations. The calculations were made for comparison with the MIR measurements over water surfaces close to the Raman lidar and rawinsonde sites at WFF. The value for T_{surf} near WFF was found to be about 296 K from the NOAA (National Oceanic and Atmospheric Administration) weekly sea surface temperature chart. The surface emissivity ϵ_s for a calm water surface could be calculated from the dielectric relaxation model for saline water (Chang and Wilheit 1979). The modification to ϵ_s caused by the surface wind speed could be made according to the model of Wilheit (1979) or Spillane et al. (1986). An examination of the rawinsonde data showed the values of surface wind speed of less than 10 m s^{-1} during the five days of the MIR measure-

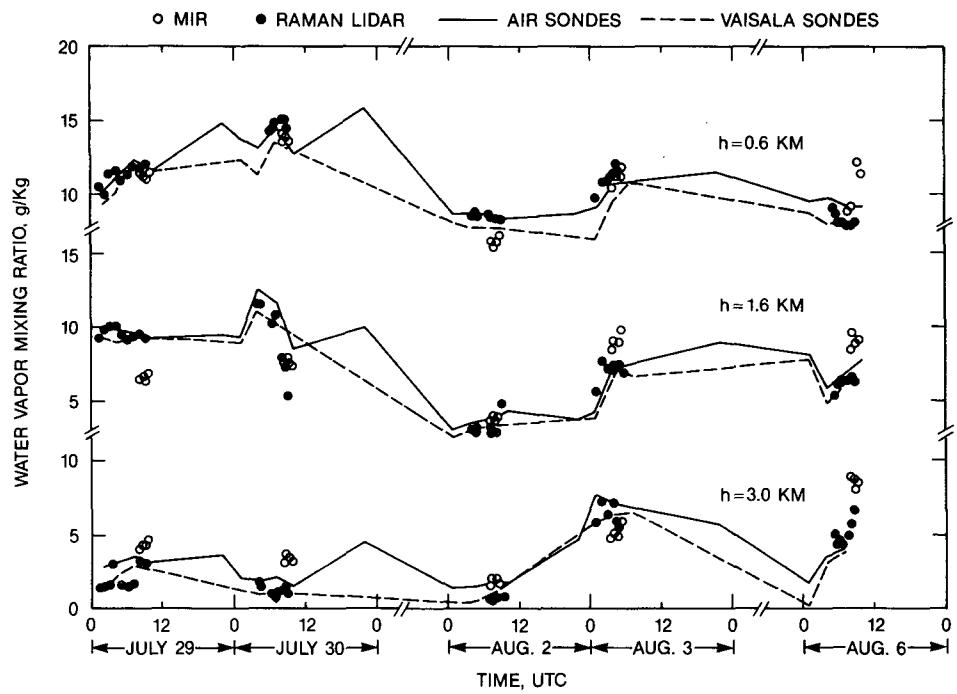

FIG. 9. A comparison of the MIR-retrieved mixing ratios with those measured by the Raman lidar, AIR sonde, and Vaisala sonde at the altitudes of 0.6, 1.6, and 3.0 km for five days in July–August 1992.

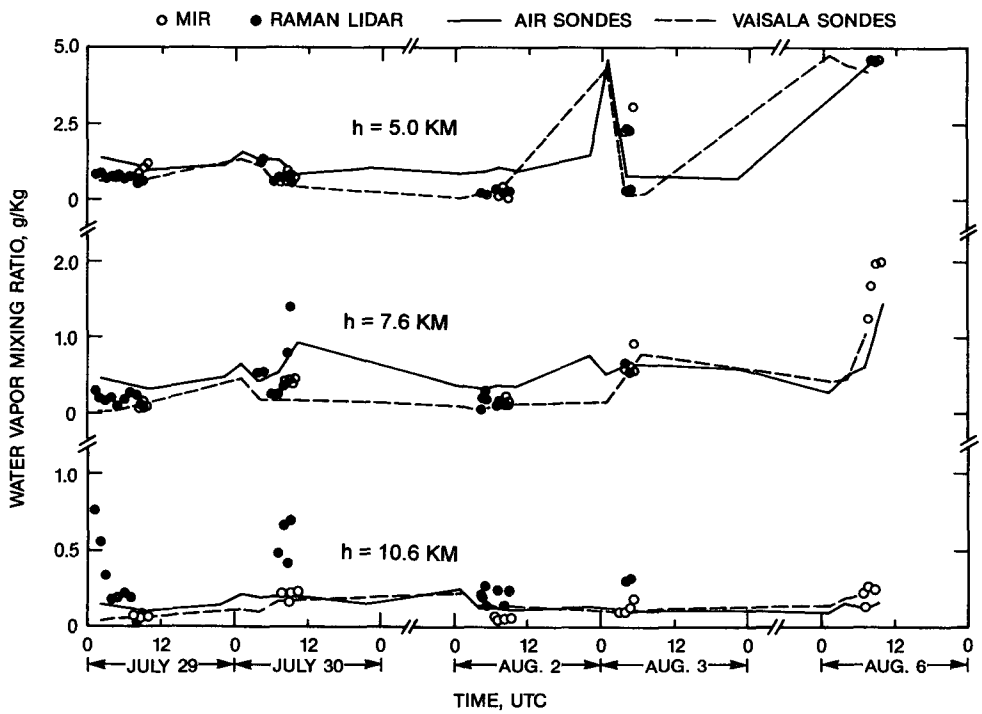

FIG. 10. A comparison of the MIR-retrieved mixing ratios with those measured by the Raman lidar, AIR sonde, and Vaisala sonde at the altitudes of 5.0, 7.6, and 10.6 km for five days in July–August 1992.

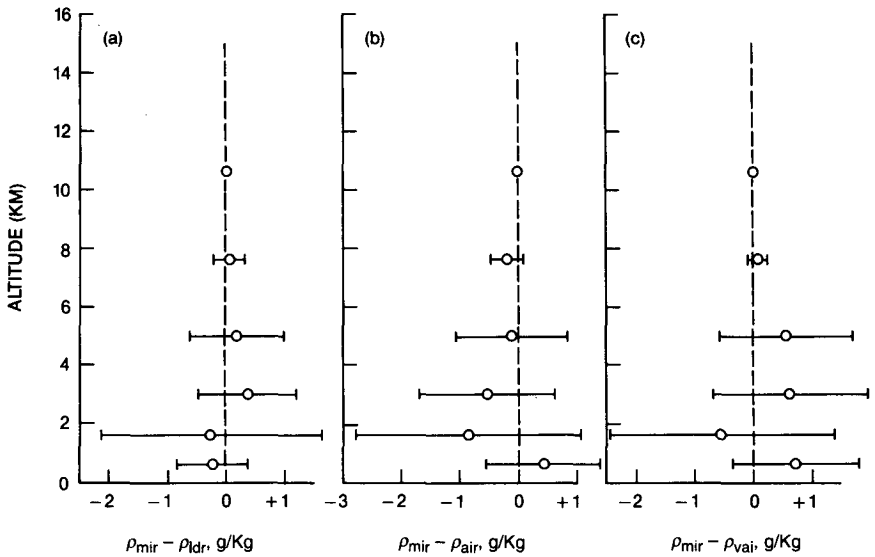

FIG. 11. Averages and standard deviations of the differences between MIR-retrieved mixing ratios and those measured by (a) Raman lidar, (b) AIR sonde, and (c) Vaisala sonde.

ments, which suggested that the modification to ϵ_s was not essential in the present calculations.

The results of radiative transfer calculations and the MIR measurements are shown in Figs. 4 and 5, respectively, for the three channels near 183 GHz and the remaining three channels at 89, 150, and 220 GHz. The figures give the variation of brightness temperature along the vertical axis and the time along the horizontal axis. The lidar measurements on the cloudy day of 6 August only covered the range from the surface to 2–3 km in altitude, and, therefore, the radiative transfer calculations based on this dataset were not made. The cloud effect was also not included in the T_b calculations from the rawinsonde observations on that day because there were no measurements of cloud liquid water content and distribution. As a result, the calculated

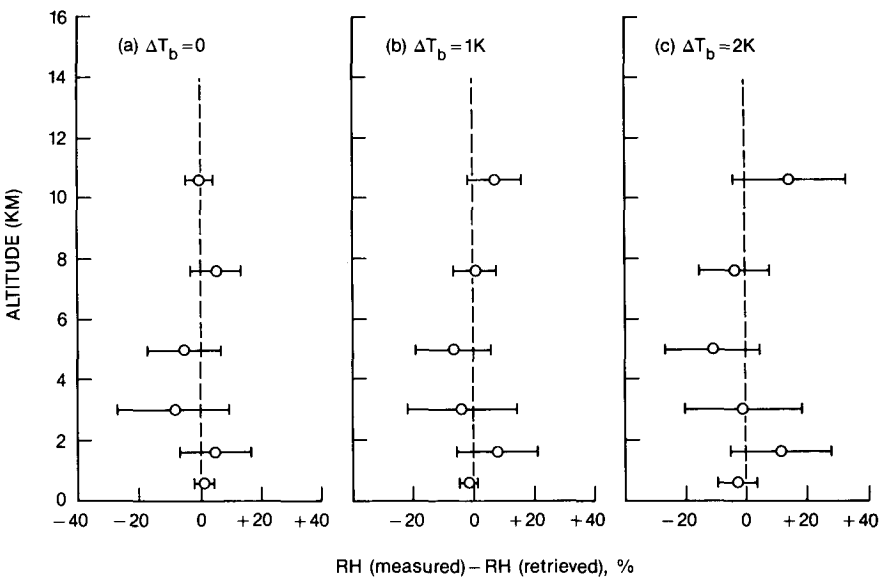

FIG. 12. Averages and standard deviations of the differences between the relative humidities retrieved from the simulated brightness temperatures and those measured by the rawinsondes. The simulated brightness temperatures were calculated from the rawinsonde measurements that include a random noise of (a) 0 K, (b) 1 K, and (c) 2 K.

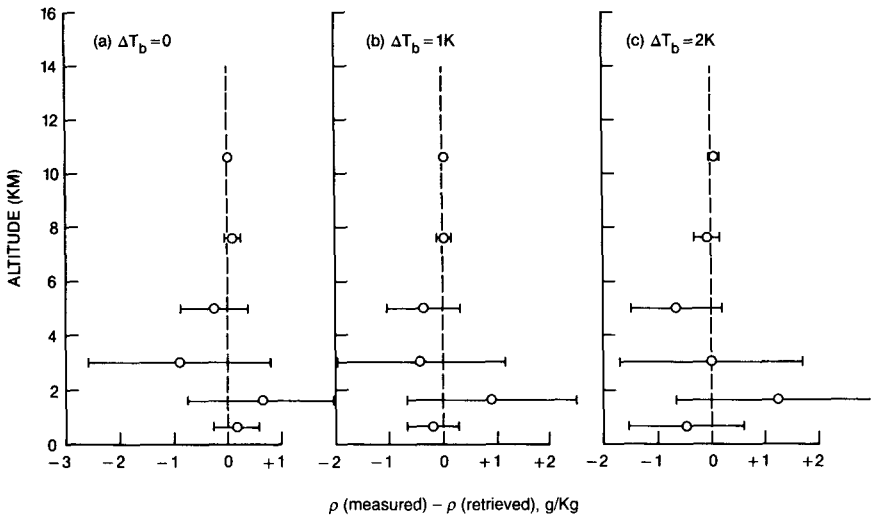

FIG. 13. Averages and standard deviations of the differences between the mixing ratios retrieved from the simulated brightness temperatures and those measured by the rawinsondes. The simulated brightness temperatures were calculated from the rawinsonde measurements that include a random noise of (a) 0 K, (b) 1 K, and (c) 2 K.

and MIR-measured T_b values for that day are not compared.

The water vapor absorption in the neighborhood of the 183.3-GHz line is well understood (Liebe 1985, 1989), and the calculated T_b values at 183.3 ± 1, 183.3 ± 3, and 183.3 ± 7 GHz should be quite accurate. It is clear from Fig. 4 that, for these three channels, results from measurements of Raman lidar and MIR are in excellent agreement. The T_b values calculated from the Vaisala sondes and the MIR measurements are also in good agreement; the largest difference being not more than 2–3 K. The T_b values derived from the AIR sonde observations, because of the sensitivity limitation at low relative humidity, differ from the others, sometimes by as much as 10 K. The calculated T_b values from the rawinsonde data for the other three frequencies at 89, 150, and 220 GHz compare much more favorably with those measured by the MIR, as shown in Fig. 5.

4. Retrieval of water vapor profiles from the MIR data

Several different retrieval techniques for water vapor profiling using the microwave radiometric measurements near 90 and 183 GHz have been explored in the past years (Wang et al. 1983; Wang et al. 1993; Kakar 1983; Kakar and Lambrigtsen 1984; Lambrigtsen and Kakar 1985; Lutz et al. 1991; Wang and Chang 1990). Other techniques have also been analyzed using simulated datasets (Rosenkranz et al. 1982; Wilheit 1990). Both approaches of Lutz et al. (1991) and Wang and Chang (1990) also allowed for an estimation of cloud liquid water at the level where the estimated relative humidity exceeded 95%. The approach of Lutz et al. employed the algorithm developed by Wilheit (1990) in his simulation studies, while that of Wang and Chang was the modified version of a Kalman–Bucy filter discussed by Ledsham and Staelin (1978) and used by Wang et al. (1983). The former gave estimated water vapor values at a few altitude levels supposedly most reflective of the radiometric measurements; consequently, the number and the altitudes of the levels might change from one location of measurements to another. The latter (Wang and Chang 1990) provided estimation of water vapor at a few selected altitude levels normally equal to the channel number of the radiometric measurements. This latter approach was used in this paper.

All six channels of MIR measurements over the ocean surface closest to the locations of Raman lidar and rawinsonde observations were used in the retrieval. The temperature profiles recorded from the Vaisala sondes at the times closest to the MIR flights were input to the algorithm. The initial input relative humidity profile was assumed to be 50% independent of altitude. The initially assumed input profile was found to have a certain impact on the finally retrieved water vapor profiles, but the effect could be minimized by tightening the convergent condition in the retrieval (Wang et al. 1994). The retrieval also adopted the same surface condition and the atmospheric millimeter-wave propagation model (Liebe 1989) described in the previous section. Six levels of retrieval were selected at the altitudes of 0.6, 1.6, 3.0, 5.0, 7.6, and 10.6 km. Typical results from the retrieval, expressed in relative humidity, were compared with those derived from the Raman

lidar and rawinsondes in Figs. 6, 7, and 8 for 2, 3, and 6 August 1992, respectively. As reflected in the rawinsonde data, the atmosphere near WFF was quite dry during the night of 2 August and modestly wet during the following night. The retrieved relative humidity profiles from the MIR measurements also suggested a more humid air on 3 August than on 2 August. There was a modest cloud cover in the proximity of WFF during the time of the measurements on 6 August. The Raman lidar measurements on that day were valid only up to the altitudes of 2–3 km and were not included in Fig. 8. The 0654 UTC AIR sonde data between the altitudes of 3.4 and 6 km were found to be erroneous, and a 100% relative humidity was assumed in the same figure.

The relative humidity profiles from the rawinsondes and Raman lidar on 2 August (Fig. 6) show a moderate broad maximum centered at the height of about 10 km and small values between the heights of 2 and 8 km. The corresponding profile retrieved from the MIR data also displays these features. On the other hand, the profiles derived from the rawinsondes and Raman lidar on 3 August (Fig. 7) show a minimum between the heights of 4 and 6 km, which is not observed from the MIR-retrieved profile. The MIR-retrieved profile also fails to show the broad maximum between the heights of 2 and 4 km that is present in both Raman lidar and rawinsonde data. This could be due to the poor vertical resolution inherent in the microwave moisture sounding—a characteristic displayed by broad peaks in the weighting functions (Schaerer and Wilheit 1979; Wang et al. 1983). The cloud cover on 6 August (Fig. 8) apparently occurred in the altitude interval of 3.5–6.0 km based on the rawinsonde data. The MIR-retrieved profile gives a 100% relative humidity in the altitude interval of 3.0–5.0 km. A total cloud liquid water of 20 mg cm^{-2} is required in the 2.0-km layer to arrive at a convergent retrieval.

The retrieved values [expressed in terms of mixing ratio ρ (g kg^{-1})] from the five days of the measurements are compared in Figs. 9 and 10, respectively, for heights at 0.6, 1.6, and 3.0 km, and for heights at of 5.0, 7.6, and 10.6 km. The Raman lidar data on 6 August and on part of 3 August are missing from Fig. 10 because the WFF was cloud covered, so that the Raman lidar range was limited to approximately 3 km above the surface. Furthermore, the Raman lidar data points at h = 10.6 km in Fig. 10 were actually measured at 9.9 km because of the limited range of the system. In general, the temporal variations of the retrieved and measured ρ values shown in these figures compare quite well.

To arrive at the statistics of the comparison between the ρ's retrieved from the MIR data and those measured by Raman lidar and rawinsondes, differences of $\rho_{mir} - \rho_{ldr}$, $\rho_{mir} - \rho_{air}$, and $\rho_{mir} - \rho_{vai}$ were tabulated and their averages and standard deviations computed. Figure 11 summarizes these averages and standard deviations at different heights. The ρ's were tagged with different subscripts for identifying mixing ratios from four different sources of MIR, Raman lidar, AIR sondes, and Vaisala sondes. For all three plots in the figure, the largest standard deviations in the differences between the MIR-retrieved ρ values and those measured by Raman lidar and rawinsondes occur at 1.6 km. This is associated with the change of the boundary layer in the 1–3-km altitudes from one day to another.

The averages and standard deviations from Fig. 11 can be compared with the magnitudes and variations of ρ's measured by any one of the three methods (Raman lidar, AIR sondes, and Vaisala sondes) during the experimental period. For example, the average values and their standard deviations of ρ_{ldr}'s for the six levels from the 0.6- to 10.6-km altitudes are calculated to be 12.36 ± 2.69, 8.29 ± 1.79, 3.87 ± 2.13, 1.24 ± 0.83, 0.35 ± 0.11, and 0.29 ± 0.15 g kg^{-1}. Figure 11 suggests that the MIR could estimate these ρ_{ldr}'s to within ± 0.66, ± 1.67, ± 1.38, ± 0.53, ± 0.35, and ± 0.09 g kg^{-1} (corresponding to percentage errors for MIR of 5%, 20%, 36%, 43%, 10%, and 31%), respectively, for the six levels from the 0.6- to 10.6-km altitudes. With the exception of the 7.6-km level, the accuracy of the estimation is better than the variation (as represented by the standard deviation) of ρ_{ldr}'s during the experimental period.

5. Discussion

The results presented in the last section showed the performance of water vapor profiling from MIR measurements with respect to the standards established by the Raman lidar and rawinsonde observations. The dependence of the retrieval results on the MIR measurement accuracy was not discussed. To explore this question, we have first made radiative transfer calculations to obtain T_b values at the MIR frequencies with eight sets of the AIR sondes and eight sets of Vaisala sondes acquired during the experimental period. Then the random noises with ΔT_b's equal to 0, 1, and 2 K were added to each set of the calculated T_b values. The resultant T_b values with random noises characterized by ΔT_b's were input to the retrieval algorithm for the estimation of relative humidities and mixing ratios at the six atmospheric levels as before. The differences between the retrieved ρ (or RH) and the measured (as derived from the respective rawinsonde datasets) values were tabulated and their averages (biases) and standard deviations of all six levels calculated. The results are summarized in Figs. 12 and 13, respectively, for the relative humidity and the water vapor mixing ratio.

Even for the ideal situation without noise input (ΔT_b = 0 K), the retrieval results from these tables show certain biases and standard deviations with respect to the truth (as represented by the rawinsonde measure-

ments). These are the intrinsic errors that cannot be avoided in the retrieval processes. The standard deviations in RH shown in Fig. 12 are rather large at the altitudes of 1.6, 3.0, and 5.0 km, the regions where the water vapor profiles measured by the AIR and Vaisala sondes at WFF show most of the rapid changes. As ΔT_b increases from 0 to 1 and 2 K, both biases and standard deviations generally show increases too, although there are some fluctuations at different levels. On the average, the increases in the standard deviations amount to about 2%–5% per 1-K change in ΔT_b. The changes in standard deviations with respect to the changes in ΔT_b's in terms of ρ can be readily observed from Fig. 13. On the average, they vary from about 0.3 g kg^{-1} at 0.6 km to about 0.04 g kg^{-1} at 10.6 km per 1-K change in ΔT_b's.

The retrieval results based on the MIR measurements summarized in Fig. 11 of the previous section can be compared with the simulated results in Fig. 13 to evaluate the performance of the instrument. First, we see that the $\rho_{\text{mir}} - \rho_{\text{ldr}}$ values in plot (a) of Fig. 11 compare favorably with those from plots (a) and (b) with $\Delta T_b = 0$ or 1 K in Fig. 13. The largest differences in these values occur at altitude $h = 1.6$ and 3.0 km; the standard deviation of $\rho_{\text{mir}} - \rho_{\text{ldr}}$ is worse at $h = 1.6$ km and better at $h = 3.0$ km than the corresponding values simulated with $\Delta T_b = 0$ or 1 K. The biases of $\rho_{\text{mir}} - \rho_{\text{ldr}}$ are somewhat better or worse, depending on h, than the simulated results. Next, the $\rho_{\text{mir}} - \rho_{\text{air}}$ and $\rho_{\text{mir}} - \rho_{\text{vai}}$ values from plot (b) and (c) of Fig. 11 are slightly worse than the simulated values with $\Delta T_b = 0$ or 1 K. They are overall somewhat better than the simulated values with $\Delta T_b = 2$ K. It was pointed out in section 3 that the AIR sondes are not sensitive at RH $< 20\%$ and Vaisala sondes tend to underestimate RH at high RH range greater than 80%. If the Raman lidar measurements are treated as the standard, then the results of these comparisons lead to the conclusion that the MIR radiometric measurements are accurate to within ±2 K. This supports the conclusion of Racette et al. (1994) on the performance of the MIR based on the laboratory measurements of external targets at known brightness temperature.

In the calculations of T_b's from Eq. (1), the surface emissivity ϵ_s was estimated from the dielectric permittivity model for a calm saline water body reported by Chang and Wilheit (1979). The effect of surface wind was assumed to be negligible during the experimental period. To estimate this effect, we can write, for a wind-roughened ocean surface, ϵ_s as a linear combination of foam and calm water fractions as

$$\epsilon_s = f\epsilon_f + (1 - f)\epsilon_w, \tag{3}$$

where f represents the fraction of sea surface that is foam covered, and ϵ_f and ϵ_w are, respectively, the emissivities of foam-covered and calm water bodies. The emissivity ϵ_w is again derived from the model of Chang and Wilheit (1979). The emissivity ϵ_f can be assumed to be equal to 1 for the worst condition. According to Spillane et al. (1986), f is related to the wind speed at a height of 10 m above the surface U_{10} by

$$f = 3.30 \times 10^{-6}(U_{10})^{3.45} \pm 8.9 \times 10^{-3}. \tag{4}$$

From the rawinsonde data obtained during the experimental period, $U_{10} \leq 10$ m s^{-1}, which suggests that $f \leq 0.01$ from Eq. (4). Therefore, the increase in emissivity caused by the wind-roughened ocean surface is at most 0.01. The retrievals using the new emissivity including the surface roughness effect show that the retrieved RH values on the average decrease by about 1.6%, which is small compared to the accuracy of the water vapor retrieval based on the microwave radiometric measurements.

Another source of error in the water vapor profiling could come from the uncertainty in the temperature profiles $T(h)$ input to the algorithm. To estimate the magnitude of this error, the input $T(h)$'s from the dry (2 August) and moist (6 August) atmospheric conditions were added to a random noise of $\Delta T(h) = \pm 1$ and ±2 K, and the retrievals repeated. A total of 15 retrievals were performed for each atmospheric condition and the resultant relative humidity profiles compared with the one derived from the original temperature profile. The bias and standard deviation were calculated at each of six altitude h levels. It was found that for both dry and moist conditions the biases in relative humidities were less than or equal to 1% at all levels and the standard deviations varied from approximately 3% to 1% for $h = 0.25$ km to $h = 10.25$ km when $\Delta T(h) = \pm 1$ K. When $\Delta T(h) = \pm 2$ K, the biases were found to be less than or equal to 2% at all levels and the standard deviations varied from about 6% at $h = 0.25$ km to 2% at $h = 10.25$ km. These results suggest that the errors in the temperature profiles are not as sensitive to the retrieved relative humidity profiles as those in the MIR radiometric measurements.

6. Conclusions

Simultaneous measurements of atmospheric water vapor were conducted with MIR, Raman lidar, and rawinsondes at NASA/Goddard Space Flight Center's Wallops Flight Facility, Wallops Island, Virginia, during 29 July–6 August 1992. A similar measurement was made previously by England et al. (1992) with the ground-based microwave radiometers at the frequencies of 20.7, 22.7, and 31.4 GHz. The water vapor line at 22.235 GHz is quite weak, and the comparison of the microwave and lidar measurements was made by these authors in terms of total precipitable water only. The newly built MIR using the strong absorption line at 183.3 GHz is capable of retrieving the water vapor mixing ratio at several altitude levels. The retrieved

mixing ratios compare favorably with those observed by Raman lidar and rawinsondes.

It was shown from radiative transfer calculations that the rawinsonde-calculated and the MIR-measured brightness temperatures could differ substantially at times. The major reason of these discrepancies is attributed to the problems associated with the rawinsonde observations of water vapor (Schwarz and Doswell 1991). One of these problems is the lack of sensitivity at the low-humidity regions experienced by the AIR sondes. This alone could make an approximate 10-K difference in the brightness temperature calculations at 183.3 ± 1 GHz as demonstrated in this paper. These problems in rawinsonde observations need to be resolved if the data are to be used regularly for validation of remote sensing instruments.

Retrieval of water vapor profiles was made from both the rawinsonde-generated (simulated) and the MIR-measured brightness temperatures. Comparisons were made between the retrieved profiles and those measured by Raman lidar, AIR sondes, and Vaisala sondes. The results from these comparisons suggest that the MIR radiometric measurements are accurate to within ±2 K and are adequate for water vapor profiling. The simulated results also show that the retrieval process degrades the accuracy of relative humidity estimation by about 2%–5% per 1-K error in the radiometric measurements. The statistics derived from the MIR-retrieved profiles are consistent with the results established by the simulation.

Acknowledgments. The authors thank Dr. R. K. Kakar, manager of NASA's Mesoscale Atmospheric Dynamics Program, for support of this experiment.

REFERENCES

Alishouse, J. C., S. A. Snyder, J. Vongsathorn, and R. R. Ferraro, 1990: Determination of oceanic total precipitable water from the SSM/I. *IEEE Trans. Geosci. Remote Sens.*, **GE-28(5),** 811–816.

Chang, A. T. C., and T. T. Wilheit, 1979: Remote sensing of atmospheric water vapor, liquid water, and wind speed at the ocean surface by passive microwave techniques from *Nimbus 5* satellite. *Radio Sci.*, **14,** 793–802.

Elliott, W. P., and D. J. Gaffen, 1991: The utility of radiosonde humidity archives for climate studies. *Bull. Amer. Meteor. Soc.*, **72,** 1507–1520.

England, M. N., R. A. Ferrare, S. H. Melfi, D. N. Whiteman, and T. A. Clark, 1992: Atmospheric water vapor measurements: Comparison of microwave radiometry and lidar. *J. Geophys. Res.*, **97**(D1), 899–916.

Falcone, V. J., M. K. Griffin, R. G. Isaacs, J. D. Pickle, J. F. Morissey, A. J. Jackson, A. Bussey, R. Kakar, J. Wang, P. Racette, D. J. Boucher, B. H. Thomas, and A. M. Kishi, 1993: DMSP F11 SSM/T-2 calibration and validation. Environmental Research Paper No. 1111, PL-TR-92-2293. [Available from Phillips Laboratory, Hanscom Air Force Base, MA 01731-5000.]

Ferrare, R. A., S. H. Melfi, D. N. Whiteman, and K. D. Evans, 1992: Raman lidar measurements of Pinatubo aerosols over southeastern Kansas during November–December 1991. *Geophys. Res. Lett.*, **19**(15), 1599–1602.

——, ——, ——, and ——, 1993: Coincident measurements of atmospheric aerosols and water vapor by a scanning Raman lidar. *Opt. Remote Sens. Atmos. Tech. Digest,* **5,** 11–14.

Garand, L., C. Grassotti, J. Halle, and G. Klein, 1992: On differences in radiosonde humidity-reporting practices and their implications for numerical weather prediction and remote sensing. *Bull. Amer. Meteor. Soc.*, **73,** 1417–1423.

Haydu, K. J., and T. N. Krishnamurti, 1981: Moisture analysis from radiosonde and microwave spectrometer data. *J. Appl. Meteor.*, **20,** 1177–1191.

Jackson, D. M., and A. J. Gasiewski, 1995: Millimeter-wave radiometric observations of the troposphere: A comparison of measurements and calculations based on radiosonde and Raman lidar. *IEEE Trans. Geosci. Remote Sens.*, **33**(1), 3–14.

Kakar, R. K., 1983: Retrieval of clear sky moisture profiles using the 183 GHz water vapor line. *J. Climate Appl. Meteor.*, **22,** 1282–1289.

——, and B. H. Lambrigtsen, 1984: A statistical correlation method for the retrieval of atmospheric moisture profiles by microwave radiometry. *J. Climate Appl. Meteor.*, **23,** 1110–1114.

Ledsham, W. H., and D. H. Staelin, 1978: An extended Kalman–Bucy filter for atmospheric temperature profile retrieval with a passive microwave sounder. *J. Appl. Meteor.*, **17,** 1023–1033.

Liebe, H. J., 1985: An updated model for millimeter wave propagation in moist air. *Radio Sci.*, **2,** 1069–1089.

——, 1989: MPM—An atmospheric millimeter-wave propagation model. *Int. J. Infrared Millimeter Waves,* **10**(6), 631–650.

Lindzen, R. S., 1990: Some coolness concerning global warming. *Bull. Amer. Meteor. Soc.*, **71,** 288–299.

Lutz, R., T. T. Wilheit, J. R. Wang, and R. K. Kakar, 1991: Retrieval of atmospheric water vapor profiles using radiometric measurements at 183 and 90 GHz. *IEEE Trans. Geosci. Remote Sens.*, **GE-29**(4), 602–609.

Melfi, S. H., and D. N. Whiteman, 1985: Observation of lower atmospheric moisture structure and its evolution using a Raman lidar. *Bull. Amer. Meteor. Soc.*, **66,** 1282–1292.

——, ——, and R. Ferrare, 1989: Observation of atmospheric fronts using Raman lidar moisture measurements. *J. Appl. Meteor.*, **28,** 789–806.

Prabhakara, C., G. Dalu, R. C. Lo, and N. R. Nath, 1979: Remote sensing of seasonal distribution of precipitable water vapor over the oceans and the interface of boundary-layer structure. *Mon. Wea. Rev.*, **107,** 1388–1401.

Racette, P., L. R. Dod, J. C. Shiue, R. F. Adler, D. M. Jackson, A. J. Gasiewski, and D. S. Zacharias, 1992: Millimeter-wave imaging radiometer for cloud, precipitation, and atmospheric water vapor studies. *IGARSS'92,* **2,** 1426–1428.

——, R. F. Adler, A. J. Gasiewski, D. M. Jackson, J. R. Wang, and D. S. Zacharias, 1994: An airborne millimeter-wave imaging radiometer for cloud, precipitation and atmospheric water vapor studies. *J. Atmos. Oceanic Technol.*, submitted.

Rosenkranz, P. W., M. J. Komichak, and D. H. Staelin, 1982: A method for estimation of atmospheric water vapor profiles by microwave radiometer. *J. Appl. Meteor.*, **21,** 1364–1370.

Schaerer, G., and T. T. Wilheit, 1979: A passive microwave technique for profiling atmospheric water vapor. *Radio Sci.*, **14,** 371–375.

Schwarz, B. E., and C. A. Doswell III, 1991: North American rawinsonde observations: Problems, concerns, and a call to action. *Bull. Amer. Meteor. Soc.*, **72,** 1885–1896.

Smith, W. L., H. E. Revercomb, H. B. Howell, H. M. Woolf, and D. D. LaPorte, 1986: The High resolution Interferometer Sounder (HIS). *CIMSS View,* **2**(3), 1–5.

Soden, B. J., S. A. Ackerman, D. O. Starr, S. H. Melfi, and R. A. Ferrare, 1994: Comparison of upper tropospheric water vapor from GOES, Raman lidar, and CLASS measurements during FIRE cirrus-II. *J. Geophys. Res.*, **99**(D10), 21 005–21 016.

Spillane, M. C., E. C. Monahan, P. A. Bowyer, D. M. Doyle, and P. J. Stabeno, 1986: Whitecaps and global fluxes. *Oceanic*

Whitecaps, E. C. Monahan and G. Mac Niocail, Eds., D. Reidel, 209–218.

Turpeinen, O. M., L. Garand, R. Benoit, and M. Roch, 1990: Diabatic initialization of the Canadian regional finite-element (RFE) model using satellite data. Part I: Methodology and application to a winter storm. *Mon. Wea. Rev.,* **118,** 1381–1395.

Wade, C. G., and D. E. Wolfe, 1989: Performance of the VIZ carbon hygrister in a dry environment. *12th Conf. on Weather Analysis and Forecasting,* Monterey, CA, Amer. Meteor. Soc., 58–62.

Wang, J. R., and L. A. Chang, 1990: Retrieval of water vapor profiles from microwave radiometric measurements near 90 and 183 GHz. *J. Appl. Meteor.,* **29,** 1006–1013.

——, J. L. King, T. T. Wilheit, G. Szejwach, L. H. Gesell, R. A. Nieman, D. S. Niver, B. M. Krupp, and J. A. Gagliano, 1983: Profiling atmospheric water vapor by microwave radiometry. *J. Climate Appl. Meteor.,* **22,** 779–788.

——, W. C. Boncyk, and A. K. Sharma, 1993: Water vapor profiling over ocean surface from airborne 90 and 183 GHz radiometric measurements under clear and cloudy conditions. *IEEE Trans. Geosci. Remote Sens.,* **31**(4), 853–859.

——, P. Racette, and L. A. Chang, 1994: MIR measurements of atmospheric water vapor profiles. *IEEE Trans. Geosci. Remote Sens.,* submitted.

Whiteman, D. N., and Coauthors, 1992a: Advanced Raman water vapor lidar. 16th Int. Laser Radar Conf., NASA Conf. Publ. 3158, Part 2, 483–484.

——, S. H. Melfi, and R. A. Ferrare, 1992b: Raman lidar system for the measurement of water vapor and aerosols in the earth's atmosphere. *Appl. Opt.,* **31**(16), 3068–3082.

Wilheit, T. T., 1979: A model for the microwave emissivity of the ocean's surface as a function of the windspeed. *IEEE Trans. Geosci. Electron.,* **GE-17,** 244–249.

——, 1990: An algorithm for retrieving water vapor profiles in clear and cloudy atmospheres from 183 GHz radiometric measurements: Simulation studies. *J. Appl. Meteor.,* **29,** 508–515.